Geomechanics and Engineering, *Vol. 11, No. 3 (2016) 401-420*
DOI: http://dx.doi.org/10.12989/gae.2016.11.3.401

Analysis of the failure mechanism and support technology for the Dongtan deep coal roadway

Miao Chen [1,2], Sheng-Qi Yang [*1], Yuan-Chao Zhang [1] and Chuan-Wei Zang [2]

[1] *State Key Laboratory for Geomechanics and Deep Underground Engineering, School of Mechanics and Civil Engineering, China University of Mining and Technology, Xuzhou 221116, P.R. China*
[2] *College of Mining and Safety Engineering, Shandong University of Science and Technology, Qingdao 266510, P.R. China*

(*Received January 21, 2016, Revised May 06, 2016, Accepted May 12, 2016*)

Abstract. The stability of deep coal roadways with large sections and thick top coal is a typical challenge in many coal mines in China. The innovative Universal Discrete Element Code (UDEC) trigon block is adopted to create a numerical model based on a case study at the Dongtan coal mine in China to better understand the failure mechanism and stability control mechanism of this kind of roadway. The failure process of an unsupported roadway is simulated, and the results suggest that the deformation of the roof is more serious than that of the sides and floor, especially in the center of the roof. The radial stress that is released is more intense than the tangential stress, while a large zone of relaxation appears around the roadway. The failure process begins from partial failure at roadway corners, and then propagates deeper into the roof and sides, finally resulting in large deformation in the roadway. A combined support system is proposed to support roadways based on an analysis of the simulation results. The numerical simulation and field monitoring suggest that the availability of this support method is feasible both in theory and practice, which can provide helpful references for research on the failure mechanisms and scientific support designing of engineering in deep coal mines.

Keywords: numerical modeling; deep coal roadway with large section and thick top coal; failure mechanism; crack propagation; combined support system

1. Introduction

Recently, deep coal roadways with large sections and thick top coal have been increasingly used by many coal mines in China with the increasing of mining depth and extensive usage of fully mechanized caving mining in thick coal seam mining (Kang 2014). These roadway often greatly deform because of the large burial depth, large sectional area and soft broken surrounding rock, which results in the failure of the bolting system. According to recent statistics, the number of roof accidents comprises more than 40% of the coal mine accidents in China. With so many deep coal roadways being built, an improved understanding of the failure mechanisms and control principles of deep coal roadways with large sections and thick top coal is essential to ensure a safe working environment for workers. Extensive research with various methods has been conducted in

*Corresponding author, Professor, E-mail: yangsqi@hotmail.com

http://www.techno-press.org/?journal=gae&subpage=7 ISSN: 2005-307X (Print), 2092-6219 (Online)

this field.

Field experiments are among the most common methods to investigate problems in deep roadways. Typical field experiments include integrated roof monitoring systems, which combine seismicity, displacement and stress monitoring to identify the roof behavior during mining-induced failure (Shen *et al*. 2008); the in-situ monitoring of zonal disintegration in deep coal mines by mine bore TV imagers (Chen *et al*. 2013); and the monitoring of the displacement, deformation convergence, bolt load, and Excavation Disturbed Zone (EDZ) of the surrounding rock (Li *et al*. 2008).

However, field experiments are limited by experimental conditions and costs (Meguid *et al*. 2008), and the results are lack repeatability and accuracy. Physical modeling tests with a small-scale model have been widely used in laboratories to investigate the failure mechanisms and reinforcement technology for roadways because the results are intuitive and easy to repeat. He (2011) and He *et al*. (2010a, b) analyzed the characteristics of excavation damaged zones (EDZ) around deep roadways in the rock strata with various inclinations by using physical model. Li *et al*. (2015) established a large-scale geomechanical model test to analyze the displacement and stress evolution laws of surrounding rock that is supported by an anchor box beam system in deep roadways.

Nevertheless, realistically simulating the in-situ stresses with physical modeling is difficult, and the production process is cumbersome with high costs. In recent years, various numerical simulations have been developed and adopted to analyze the stability of surrounding rock in deep roadways because of their low cost and high efficiency. Current numerical approaches can be classified into continuum-based and discontinuum-based methods (Jing and Hudson 2002, Jing 2003). Two main representative methods exist: finite element methods (FEM) and discrete element methods (DEM).

The discontinuity of rock materials (such as joints, cracks, bedding and different mineral compositions) cause continuum mechanics to exhibit significant deficits. Discrete mechanics are rapidly becoming more popular because DEMs can represent broken states and the strong nonlinear mechanical phenomena of surrounding rocks in deep coal mines. Boon *et al*. (2015) used DEMs to analyze the failure patterns for unsupported openings and the effect of different support parameters on the tunnel convergence. Karampinos *et al*. (2015) employed the 3DEC model to simulate the buckling mechanisms in deep and high-stress hard rock mines. Gao *et al*. (2014a, b) studied roof shear failure and squeezing failure in roadways by using the UDEC's trigon approach. Shen (2014) and Kang *et al*. (2015) applied the UDEC to simulate the failure mechanism and new support designs for roadways in soft rock. The simulation results matched well with field situations, which indicate the reliability and practicability of DEM in simulating deep coal roadways. Further research is required on the failure mechanisms and support technology in deep coal roadways because of their complex geological conditions.

In this paper, numerical modeling on the failure mechanism and support technology in a deep coal roadway is performed with the trigon block in the UDEC. A detail numerical model is first established by trigon blocks based on a case study of Dongtan coal mine, and the parameter calibration process is also illustrated. A simulation of an unsupported roadway is then performed to investigate the excavation-induced displacements, stresses and failure mechanisms. Finally, stability control mechanisms and support technology for the roadway are proposed and used to support the roadway. Simulations and field tests are also conducted to evaluate the control effect of a combined support system on the surrounding rock along the roadway.

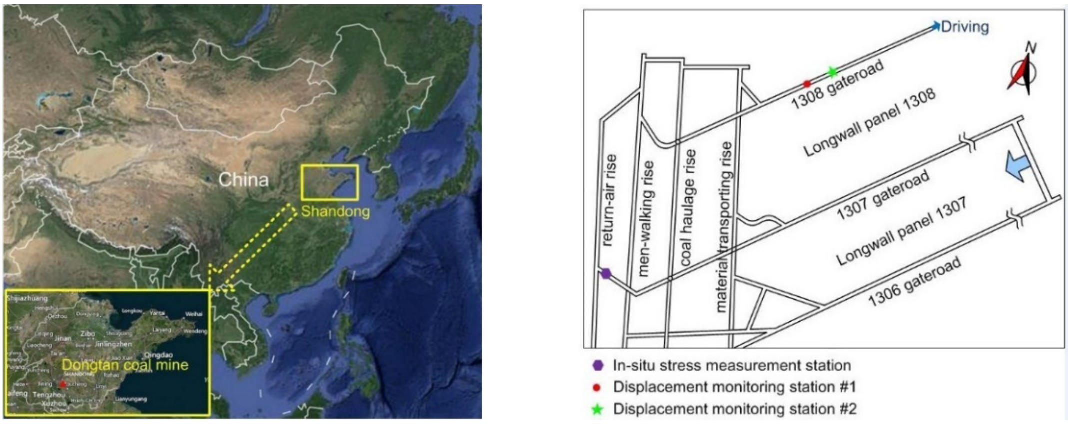

(a) (b)

Fig. 1 (a) Location of the Dongtan coal mine, Shandong, China; (b) Plan view of the gate-road and panel at the study site in the Dongtan coal mine

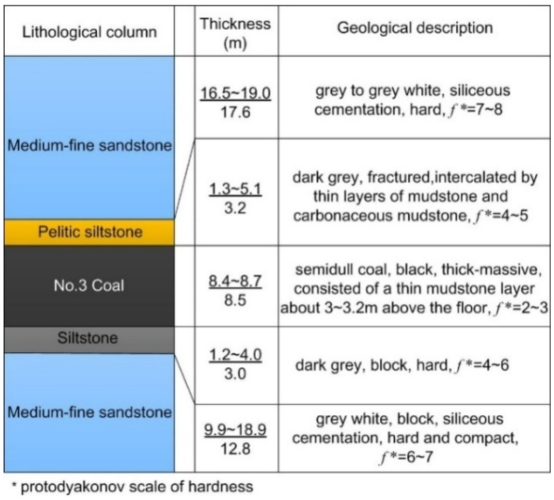

Fig. 2 Lithological descriptions of the rock strata at the1308 gate-road

2. Engineering geological conditions

The Dongtan coal mine is located in the east-central Yanzhou coal mining district in China's Shandong province (Fig. 1(a)). The 1308 workface is situated to the north of the No. 1 mining area at a mining depth of approximately 600 m. The upper 1309 workface has not yet been mined out, and the lower 1307 workface is being extracted with a fully mechanized caving method (Fig. 1(b)). The mining seam has a height of 8.5 m; above the coal seam is a pelitic siltstone with a thickness of 3.2 m, and the main roof is relatively competent medium-fine sandstone with a thickness of 17.6 m. The immediate floor is a hard integrated siltstone with an average thickness of 1.3 m, and underlying this stratuma is a medium-fine sandstone with a thickness of 12.8 m. Detailed lithological descriptions of the rock strata are illustrated in Fig. 2. The 1308 gate-road, which has

Table 1 Physical-mechanical parameters of the intact rock at the Dongtan coal mine

Lithology	Elastic moduli (GPa)	Poisson's ratio	Density (kg/m^3)	Friction angle (°)	Cohesion (MPa)	Compressive strength (MPa)
Medium-fine sandstone	5.4	0.25	2560	31	30.2	55
Pelitic siltstone	3.6	0.235	2480	31.3	4	30.2
No. 3 Coal	1.4	0.29	1400	30	3.5	8.5
Siltstone	4.1	0.22	2560	27	8	32

dimensions of 5.2 m × 4 m, is driven along the immediate floor.

In-situ stress measurements by hydraulic fracturing were recorded in the location of return-air rise near the 1308 workface. The results are $\sigma_{h\max}$ = 18.73 MPa, $\sigma_{h\min}$ = 11.12 MPa, and σ_v = 12.19 MPa, and the direction of $\sigma_{h\max}$ is 47°. Therefore, the horizontal stress has little effect on the roadway because the angle between the maximum principle stress and the 1308 gate-road is 5° (nearly parallel). The physical-mechanical parameters of the intact rock, which were provided by Dongtan coal mine, were obtained though laboratory compressive tests and are listed in Table1 (Meng 2013).

3. Discrete element method simulation

3.1 UDEC trigon method

The Universal Distinct Element Code (UDEC) is used because it can better simulate the broken status of surrounding rock in deep coal mines. The computational domain in the UDEC is discretized into blocks by using a finite number of intersecting discontinuities (Itasca 2004). The discontinuities are treated as boundary conditions between blocks. Large displacements that are caused by the rigid body motion of individual blocks, including block rotation, fracture opening and complete detachments, are straightforward in the UDEC. Individual blocks behave as either rigid or deformable material. The motion of a block is described by Newton's second law of motion under disturbance forces from applied loads, body forces and forces from adjacent blocks.

The shapes of surrounding rock in deep roadways are usually irregular, but most of the traditional simulation methods that used regular blocks had difficulty simulating the real structural features and dynamic mechanical behavior of surrounding rock.

The trigon blocks are generated based on the Voronoi algorithm in UDEC with the custom-developed FISH function, which could cut Voronoi blocks into several constituent trigon blocks (Gao and Stead 2014). In the trigon approach, a rock mass is represented as assemblages of trigon blocks that are formed by connected fractures in the numerical model; the fracture process can be represented by the sliding or opening of the contact between trigon blocks. In this paper, the elastic constitutive model is used for blocks and the coulomb slip model is used for contacts. The deformation and mechanical behaviors of the numerical model depend on the micro mechanical parameters of the trigon blocks and its contacts (Christianson *et al*. 2006), as shown in Fig. 3.

Previous studies (Kazerani 2013, Kazerani and Zhao 2010) concluded that the deformation characteristics of trigon blocks are affected by the bulk moduli (K) and shear moduli (G); the deformation characteristics of contacts are characterized by the normal stiffness (k_n) and shear stiffness (k_s) of the contacts, while the strength characteristics of the contacts are characterized by

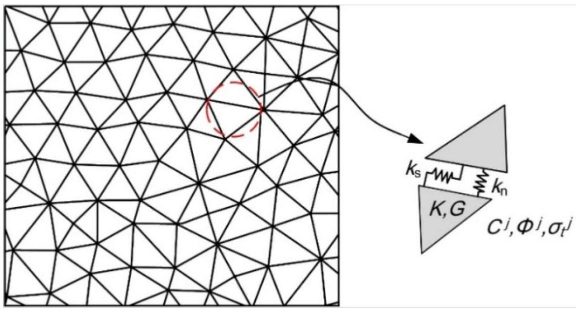

Fig. 3 Trigon model with the contact parameters marked

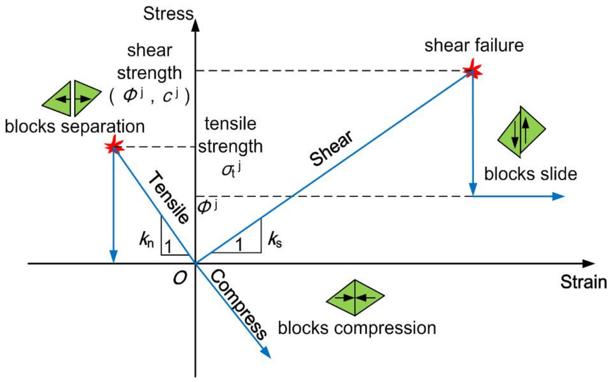

Fig. 4 Constitutive model of a trigon block contact (Kazerani 2013, Kazerani and Zhao 2010)

the cohesion (C^j), friction angle (Φ^j) and tensile strength (σ_t^j) of the contacts. A constitutive model of the contacts is shown in Fig. 4. Model deformation occurs when the contact stress is smaller than the contact strength, which is governed by the deformation moduli and contact stiffness; contact failure occurs when the stress exceeds its strength, and slide and separation occur in the adjacent blocks.

3.2 Calibration of micro-parameters

Parameter determination is one of the fundamental aspects of numerical simulations, especially for discontinuum mechanics analytical method. The mechanical parameters of the intact rock from the 1308 gate road are listed in Table 1. However, a rock mass is the synthesis of intact rocks and fissures, and differences exist between the mechanical parameters of intact rock and rock masses. Zhang and Einstein (2004) analyzed field and laboratory date and determined a relationship between the rock quality design (RQD) and the ratio of the deformation moduli between a rock mass and an intact rock specimen.

$$\frac{E_m}{E_r} = 10^{0.0186RQD} - 1.91 \tag{1}$$

where E_r and E_m are the deformation moduli of intact rock and a rock mass, respectively.

Singh and Seshagiri (2005) summarized field tests, and obtained a correlation between the ratio of the uniaxial compressive strength between a rock mass and a rock specimen and the ratio of the deformation moduli between a rock mass and a rock specimen.

$$\frac{\sigma_{cm}}{\sigma_c} = \left(\frac{E_m}{E_r}\right)^n \tag{2}$$

where σ_c and σ_{cm} are the uniaxial compressive strength of an intact rock and a rock mass, respectively; n was set to 0.63 (Singh and Seshagiri 2005).

The parameters of the rock mass (Table 2) are obtained from the intact rock parameters (Table 1) by using formulas (1) and (2). The RQD values are obtained by using a borehole camera in the 1308 gate-road in the Dongtan coal mine, and the tensile strength of the rock mass is estimated to be 10% of the compressive strength.

Table 2 Physical mechanical parameters of the rock mass in the Dongtan coal mine

Lithology	RQD	E_m (GPa)	σ_{cm} (MPa)	σ_t (MPa)
Medium-fine sandstone	89	3.00	38.02	3.80
Pelitic siltstone	76	1.15	14.70	1.47
No. 3 Coal	71	0.36	3.61	0.36
Siltstone	83	1.69	18.31	1.83

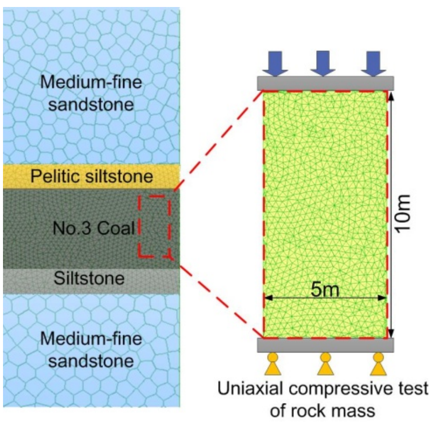

Fig. 5 Diagram of the calibration test

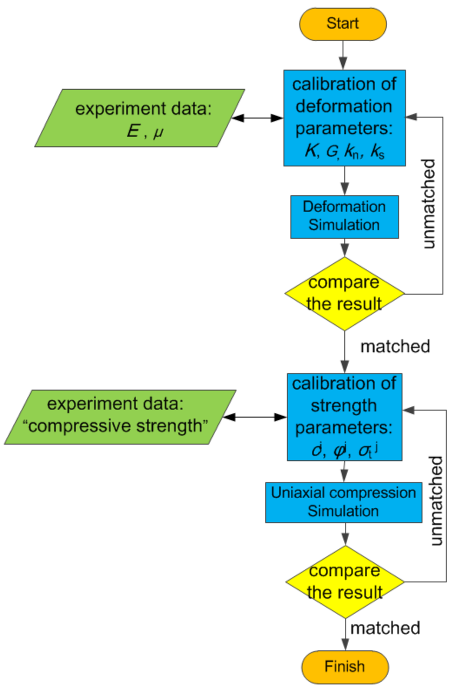

Fig. 6 Micro-parameter calibration process (Tan and Konietzky 2014)

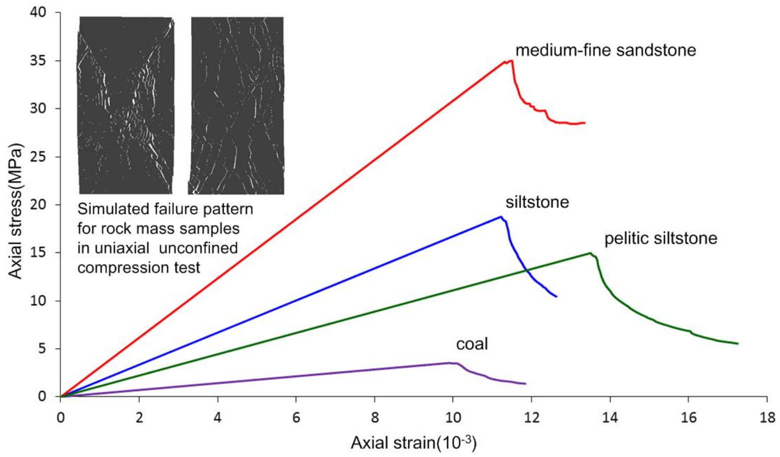

Fig. 7 Simulated uniaxial stress-strain curves for the rock masses with the micro-parameters in Table 3

The micro-parameters of blocks and contacts that are required in the UDEC cannot be directly obtained from physical mechanical parameters. In this paper, a series of simulated compression tests with trigon blocks are conducted to calibrate the micro-parameters of the blocks and contacts (Gao *et al*. 2014a). The numerical model has a larger block size and model size while keeping the length-to-width ratio constant to eliminate the influence of the mesh size, as shown in Fig. 5. The original macro-parameters are first assumed according to the material's characteristics, and then uniaxial compression numerical tests and analysis are performed iteratively until the simulation test results were consistent with the micro-parameters of the rock mass. The calibration test method in this paper is shown in Fig. 6. Fig. 7 shows the simulated fracture patterns and stress-

Table 3 Calibrated micro-parameters for the rock mass

Lithology	Matrix properties		Contact properties				
	Density (kg/m^3)	E (GPa)	k_n (GPa/m)	k_s (GPa/m)	C^j (MPa)	Φ^j (°)	σ_t^j (MPa)
Medium-fine sandstone	2560	3.04	333.0	133.0	9.0	36	3.80
Pelitic siltstone	2480	1.11	134.0	53.6	6.5	36	1.47
No. 3 Coal	1400	0.35	65.8	26.3	1.6	33	0.36
Siltstone	2560	1.63	209	83.6	7.2	34	1.83

Table 4 Comparison between the targeted and simulated Young's moduli and compressive strengths

Lithology	E_m (MPa)		Error (%)	σ_{cm} (MPa)		Error (%)
	Target	Simulation		Target	Simulation	
Medium-fine sandstone	3.00	3.04	-1.3	38.02	34.98	-8.0
Pelitic siltstone	1.15	1.11	-3.5	14.70	14.94	-1.6
No. 3 Coal	0.36	0.35	-2.8	3.61	3.53	-2.2
Siltstone	1.69	1.63	-3.6	18.31	18.16	-0.8

strain curves for the rock mass from the compression test samples; the final simulation parameters for the rock mass are listed in Table 3. Comparisons of the targeted and calibrated Young's moduli and compressive strengths are presented in Table 4. These comparisons show that calibrated Young's moduli and compressive strength have good consistency with the targeted values. Therefore, the micro-parameter list in Table 3 could be applied to the stability simulations of the surrounding rock along roadways because the mechanical behaviors of the assembly of trigon blocks are consistent with those of the rock mass.

3.3 Simulation model establishment

A numerical model of the 1308 gate-road is created by using trigon blocks in the UDEC. Fig. 8 shows the geometry of the model, which is based on the lithology of the 1308 gate-road as illustrated in Fig. 2 and Table 3. The main aim of this study is to investigate the behavior of the rock mass that surrounds the roadway, which was created by excavation. Trigon blocks are only generated in the area of interest that surround the 1308 gate-road to increase the computational efficiency; the remainder of the model is still divided into Voronoi blocks. The average edge length of the trigon blocks in the coal seam is set to 0.2 m, and trigon blocks with an average edge length of 0.5 m are used to simulate pelitic siltstone and siltstone in the areas of interest. The edge length of the Voronoi blocks in the coal seam, immediate roof and immediate floor is set to 1 m, and the average length in the main roof and main floor is set to 2 m. A graded increasing edge length is used to avoid a sudden large increase in the block size, enhancing the calculation's accuracy.

The horizontal displacement is constrained along the lateral boundaries of the model, and the vertical and horizontal displacements are fixed at the bottom boundary. The roadway could regarded as plane strain model in the axial direction. The in-situ stresses are applied to the boundaries to construct the initial rock stress field. The model is run to equilibrium to generate the in-situ stress before the roadway was excavated by deleting the block to simulate the excavation.

A roadway is usually excavated by using a heading machine, and the deformation of the surrounding rock around the roadway is confined by the excavation face (Brady and Brown 2006). Li *et al*. (2015) found that the stress redistribution of the surrounding rock shows a step-type

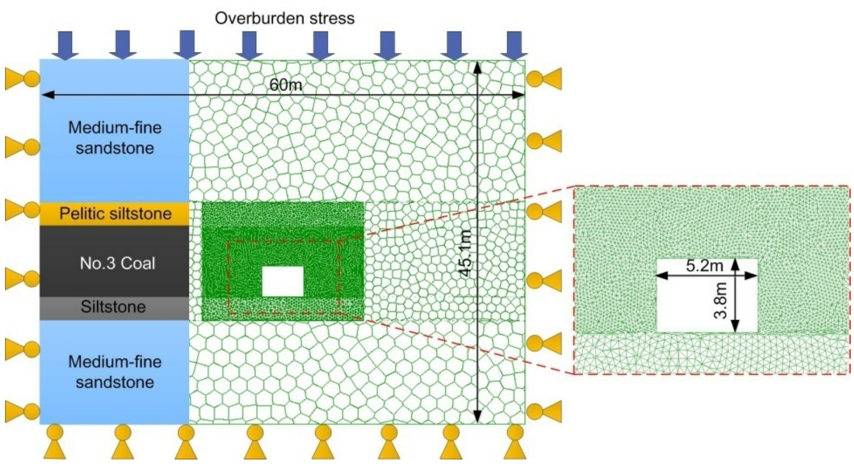

Fig. 8 Numerical model for the surrounding rock of a large road way section with thick top coal in a deep mine

decreasing trend as the deep rock mass is excavated based on the results of similarity model tests. Therefore, the Fish function “ZONK.FIS” in the UDEC (Itasca 2004) is used to simulate the realistic process of stress relief. The stresses that are applied to the roadway surface decrease from 100% to 0% in 10% decrements after ten stages(designated I, II, III, IV, V, VI, VII, VIII, IX and X).

4. Numerical Results Analysis

4.1 Displacement analysis

The surrounding rock could reach a new equilibrium by deformation and stress adjustment after excavation. Four monitoring lines are placed in the middle of the roof, floor and sides to record changes in the displacement and stress in the surrounding rock to analyze the effect of the excavation on the surrounding rock. Fig. 9 shows the displacement curves of the monitoring points at the roadway surface after excavation. Fig. 10 shows the displacement curves of the roof, floor and sides at different depths. Fig. 11 shows a displacement vector map of the surrounding rock. The deformation law of the surrounding rock could be summarized as follows according to the monitoring results.

(1) The displacement curves of the monitoring points at the roadway surface show a step-type increasing trend, which reveals that the relief degree of the stress had a larger effect on the deformation of the surrounding rock. The deformation process from stage I to stage X showed that the stress relief accelerated the deformation process in the surrounding rocks, and a critical deformation value existed for each stage. The deformations of the surrounding rock were within the controllable range before the stress decreased to stage X, but deformation was greatly accelerated when the stress decreased from stage XI to stage X. The deformations in the roof, sides and floor at stage X were 788 mm, 609 mm and 49 mm, and the growth rates were 219.0%, 74.0% and 17.1% higher than those at stage IX, respectively.

(2) The final deformation curves show that roof subsidence was the main form of deformation in the surrounding rock and was obviously larger than that in the sides and floor. The deformations in the surrounding rock was mainly concentrated within 5 m from the roadway surface and gradually reduced from shallow to deep areas. The displacement of

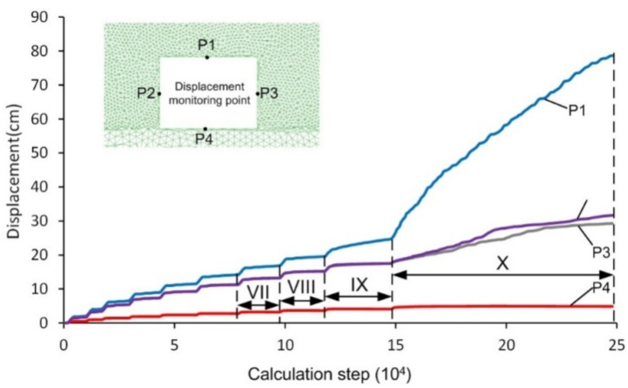

Fig. 9 Displacement curves of the monitoring points at the roadway surface after excavation

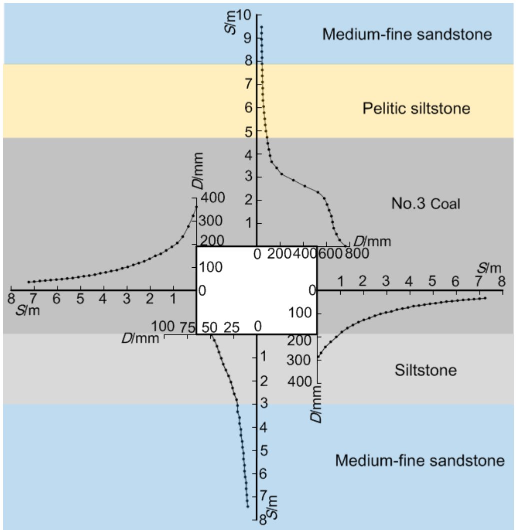

Fig. 10 Simulated displacements in the roof, floor and sides at different depths under unsupported conditions

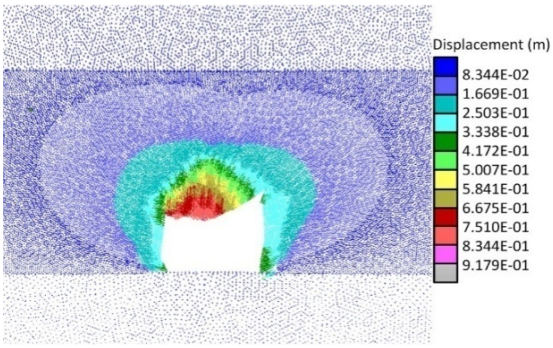

Fig. 11 Simulated displacement vector map of the surrounding rock along the roadway under unsupported conditions

the surrounding rock between 2 m to 3.7 m from the roof reached 480mm, which comprised 65% of the total displacement. This sudden increase in the displacement indicates that roof separation may have occurred in this area.

(3) The displacement vector map indicates that the excavation caused uneven deformation in the surrounding rock. Vertical displacement from gravity was the main deformation form in the roof, and the subsidence in the center of the roof was larger than on both of the sides. Horizontal displacement was predominant in the deformation along the sides; the convergence of the roadway along the sides was approximately 0.6 m, and the displacement in the side corner was larger than that in other areas. Little floor heaving occurred because of the hard nature of the immediate floor.

4.2 Changing stress features in the surrounding rock

The excavation of the roadway redistributed the stress in the surrounding rock. The stress release rate was introduced to describe the characteristics of the stress distribution, namely, the percentage of the stress reduction in stable surrounding rock after excavation compared to the in-situ stress, to clearly explain the stress changes in our model (Li *et al*. 2015).

$$\lambda = \frac{\sigma_m - \sigma_n}{\sigma_m} \times 100\% \tag{3}$$

where λ is the stress release rate (%), and σ_m and σ_n are the in-situ stress and stress after the excavation of the surrounding rock, respectively.

Fig. 12 demonstrates the stress release rates that were calculated based on the monitoring results of four monitoring lines in the roof, floor and sides. The positive λ values indicate stress reduction and negative values indicate stress concentration. Similar isolines of the vertical and horizontal stress release rate at 25%, 50% and 75% were plotted in Fig. 12. The main conclusions on the stress monitoring results are as follows:

(1) In general, the stress release rate reduced from 100% to 0% with distance away from the roadway surface: the farther the position from the roadway surface, the smaller the disturbance on the in-situ stress became. The stress release rate of the vertical stress in the roof and floor and the horizontal stress in the sides (similar to the radial stress around the roadway) decreased with increasing distance from the roadway surface. Meanwhile, the stress release rate of the horizontal stress in the roof and floor and the vertical stress in the sides (similar to the tangential stress) first decreased to negative values and then increased to 0, which indicates that the deep surrounding rock of the roadway bore more tangential stress within a certain range, while the region outside this increasing tangential stress zone was the in-situ stress zone. At the same time, horizontal stress release zones only appeared within a small range along the floor because of the hard siltstone floor.

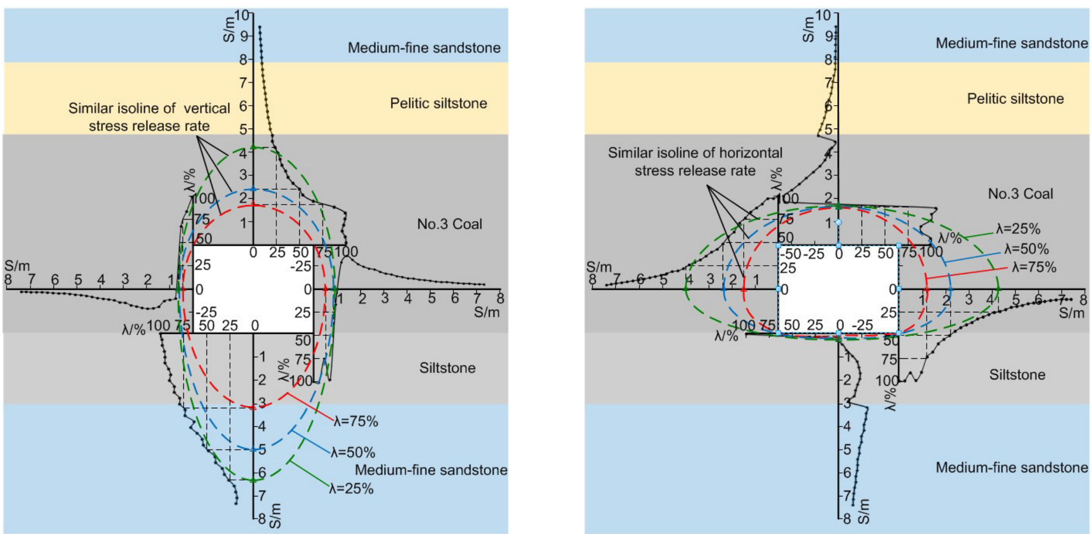

(a) Vertical stress release rate (b) Horizontal stress release rate

Fig. 12 Simulated stress release rate of the surrounding rock at different depths under unsupported conditions

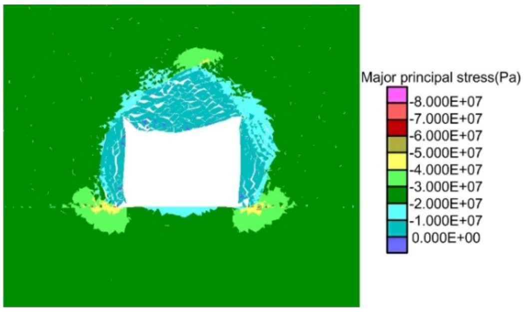

(a) Major principal stress distribution

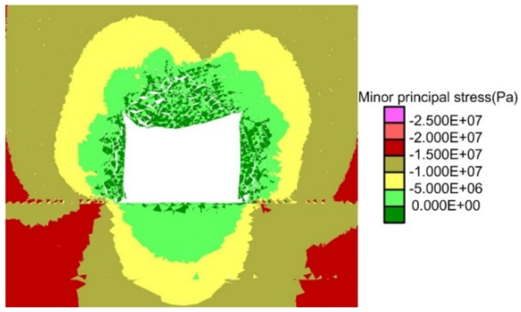

(b) Minor principal stress distribution

Fig. 13 Simulated principal stress distribution around the 1308 gate-road under unsupported conditions

(2) The similar isolines of the vertical stress release rate approximated a “thin oval”, which is tall in the vertical direction and narrow in the horizontal direction and shows that the vertical stress that was released in the roof and floor was more severe than that in the sides, easily leading to roof fall and floor heaving. Meanwhile, the similar isolines of the horizontal stress release rate approximated a “flat oval”, which shows that the horizontal stress that was released along the sides was more severe than that in the roof and floor, easily leading to rib spalling.
(3) Principal stress distribution: Fig. 13(a) shows that the surrounding rock was generally under compression; high stress concentration zones with small ranges occurred in the bottom corners and 2 m above the roof, while decreasing stress zones occurred in the roof and sides over a large range. Interestingly, the decreasing stress zones had similar ranges with the loosening zones (the area where the displacement exceeded 0.25 m, see Fig. 11). Fig. 13(b) illustrates that the areas near the roadway surface exhibited larger tensile stress from excavation.

4.3 Failure process analysis

Many engineering practices have proven that the instability of the surrounding rock in underground engineering is closely related to the propagation of cracks (Yang 2015) and that the excavation of roadways would facilitate the propagation of cracks. The crack propagation of the surrounding rock after excavation is captured in the UDEC, as shown in Fig. 14, to obtain the propagation law of cracks. The cracks are marked by black lines, while the intact rock is colored yellow (Fig. 14). The failure processes of the surrounding rock can be classified into the following four stages based on the characteristics of the crack propagation:

(1) As the stresses that were applied on the surrounding rock gradually decreased after excavation, the stress concentrated in the four corners because of the poor force state of the rectangular cross-section. Small cracks occurred in the corners when the stress that was applied on the rock exceeded the compressive strength (Fig. 14(a)).
(2) Large-scale tension stress zones occurred in the shallow roof under the action of gravity when the stress decreased to stage VI, and cracks in the roof propagated from the corners to depth in an arc shape, which formed a 1.4 m high arc-shaped fracture zone, while the amount of cracks only increased slightly in the corners during this stage, (Fig. 14(b)).

(3) When the stress decreased to stage IX, part of the overburden stress that was applied on the roof transferred to the roadway sides because of roof failure. Cracks along the sides extended inward from the corners in an arc shape under the action of vertical and horizontal pressure. The cracks in the roof extended deeper into the top coal creating a 2-m-high triangular distribution. The cracks in the bottom corners extended along the bedding plane (Fig. 14(c)).

(4) When the stress was entirely released, the failure along the sides increased the roadway's span, which accelerated roof failure and led to a vicious circle. Cracks in the roof and sides greatly developed and formed a fracture zone that was 2.3 m high above the roof and 2 m long outside the sides (Fig. 14(e)). As the cracks continued to propagate and interact, the shallow coal began to separate from the surrounding rock, which would increase the instability of the roadway if efficient support measures are not adopted. Fig. 15(a) illustrates the final failure pattern: collapse in the roof and rib spalling in the sides. The numerical results agree well with the field result (Fig. 15(b)). The floor remained stable because of the hard siltstone floor.

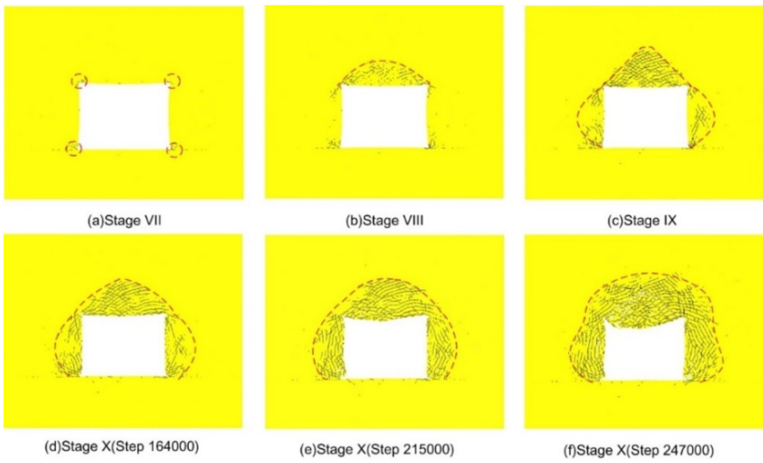

Fig. 14 Propagation of cracks in the surrounding rock along the roadway after excavation without support

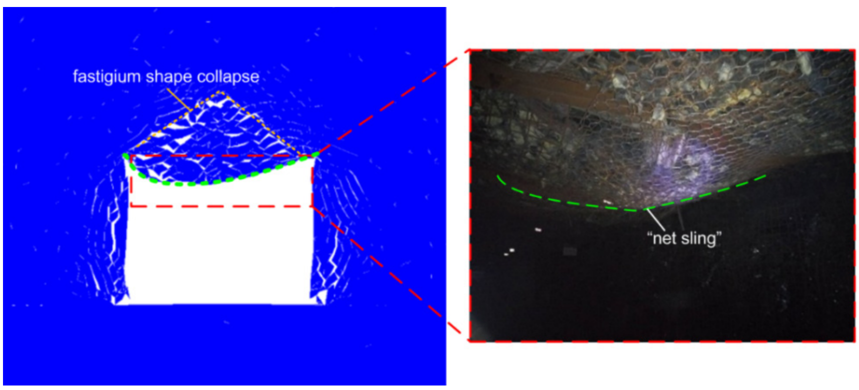

(a) Simulated failure patterns (b) Field photo of the "net sling"

Fig. 15 Simulated failure patterns and an example of "net sling" in the field

5. Surrounding Rock Control Technology

5.1 Control principle of the surrounding rock

The failure process of the surrounding rock along the roadway shows that stress release in the surrounding rock can decrease the confining pressure and increase the deviator stress, while the strength of the surrounding rock decreases. Roof failure occurred first, and then the stress state along the sides deteriorated, which accelerated the instability process. The important area that must be well supported is the roof, and the confining pressure should be increased to improve the strength of the surrounding rocks and decrease deformation. The support design criteria for deep coal roadways with large sections and thick top coal are proposed as follows:

(1) Immediate high pre-stressed support: Research shows that the residual strength of rock specimens under low confining pressure increases greatly as the confining pressure increases (Yang *et al*. 2008; Jing *et al*. 2014), which means that the residual strength is sensitive to the confining pressure. Bolts and cables should be supported in time, and enough pre-stress should be exerted to improve the surrounding pressure of the surrounding rock, which could increase the initial supporting stiffness and strength of the bolting system to maintain the integrity and reduce any decreases in strength in the surrounding rock.

(2) Combined support: Common short anchor bolts cannot control large fracture zones in thick top coal because of the soft and broken features of roof coal. Therefore, high-strength, strongly anchored long cables should be used to suspend the shallow top coal in the upper hard middle-fine sandstone, which increases the resistance of deeper surrounding rock and prevents the top coal bed from separating. Wire mesh with a roof channel for surface support could improve the loading states and prevent damage from developing in deeper areas. Bolts near the corners should be set at an angle to form an integral anchorage structure to improve the stress concentration, which can easily appear in these corners.

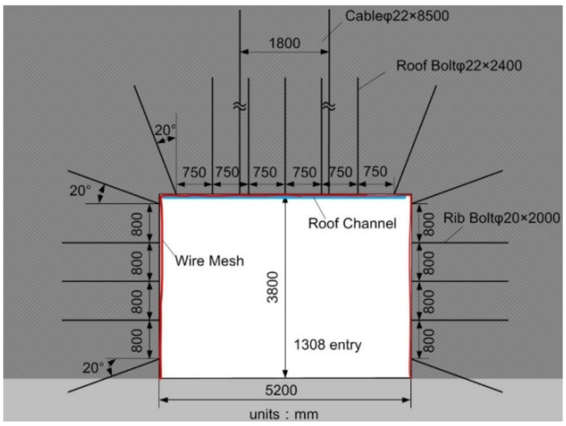

(a) Plan view

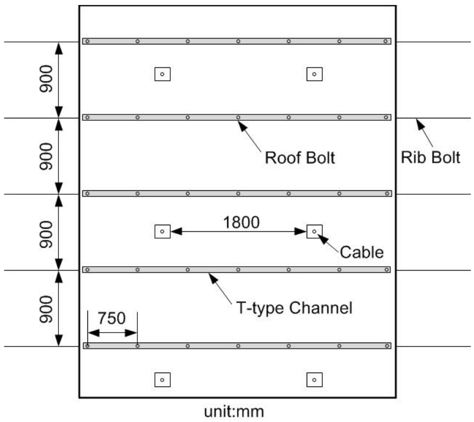

(b) Top view

Fig. 16 The anchor bolt-cable-channel-mesh combined support system for the 1308 entry

Table 5 Properties of the support elements in UDEC

	Fish language	Density /kg·m^{-3}	Elastic moduli /GPa	Tensile yield strength /kN	Bond stiffness /GPa	Bond strength /MPa	Pretension /kN
Roof bolt	Cable	7500	200	220	3	6	85
Side bolt		7500	200	185	3	6	85
Cable		7500	200	500	5	10	180
Channel	Struct	7500	200	500	10	10	-

5.2 The combined support scheme

According to the above analysis, an anchor bolt-cable-channel-mesh combined support scheme is proposed as follows. Seven Φ22 mm×2400 mm high-strength bolts are installed in the roof with a pretension of 85 kN, and five Φ20 mm×2000 mm bolts are installed in each side with a pretension of 85 kN, with each bolt installed with a 150 mm×150 mm×10 mm load-bearing plate. Two Φ22 mm×8500 mm high-strength cables are installed with a pretension of 180 kN, and each cable is installed with a 250 mm×250 mm×18 mm load-bearing plate. Roof bolts and cables are installed with a T-type channel that is 4.8 m long and a wire mesh with a grid size of 50 mm×50 mm. Details of the support parameters are shown in Fig. 16. This combined support system is adopted in the UDEC to analyze the supporting effect. The parameters of the support elements that were used in the UDEC are presented in Table 5.

5.3 Effect analysis of the combined support system

The deformation in the surrounding rock was significantly reduced by the combined support system. The displacement along the roof and sides was 450 mm and 420 mm, respectively, compared to 788 mm and 609 mm in the unsupported roadway, a reduction of approximately 42% and 30%, respectively (see Fig. 17).

The displacement vector of the surrounding rock along the roadway with the combined support system is shown in Fig. 18; the deformation range was significantly reduced because of the application of this combined support system. Compared to that in an unsupported roadway, the deformation tended to be more uniform with no significant sliding or collapses in the surrounding rock, which demonstrates the coordination of the support system and the surrounding rock.

Compared to that in an unsupported roadway, the distribution trend of the principal stress in the surrounding rock under supported conditions did not change remarkably, as shown in Fig. 13 and Fig. 19. However, a comparison shows that the tensile zone significantly decreased; thus, the combined support system can greatly improve the state of the stress distribution in shallow surrounding rock.

Fig. 20 shows the simulated crack distribution of the 1308 gate-road with the combined support system. The fractured zone of the surrounding rock along the roadway decreased dramatically; in particular, the cracks in the roof and sides were not connected in the top corners. The support elements were all in tension because of the restriction of the swelling deformation in the surrounding rock, as shown in Fig. 21. The cable’s high bearing capacity enhanced the stability of the top coal by increasing the resistance of deeper surrounding rock.

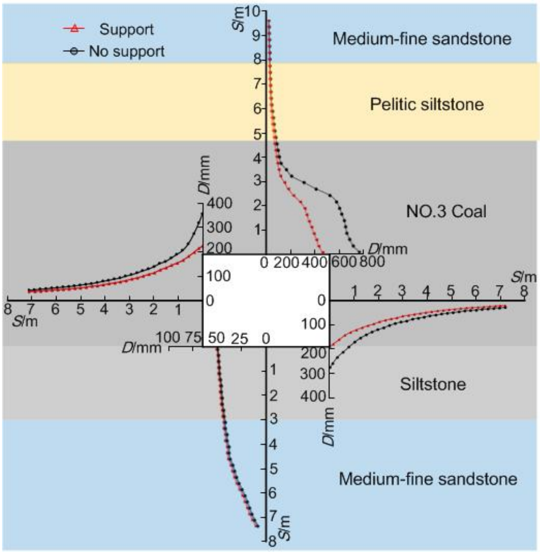

Fig. 17 Control effect of the combined support system in the surrounding rock along the roadway

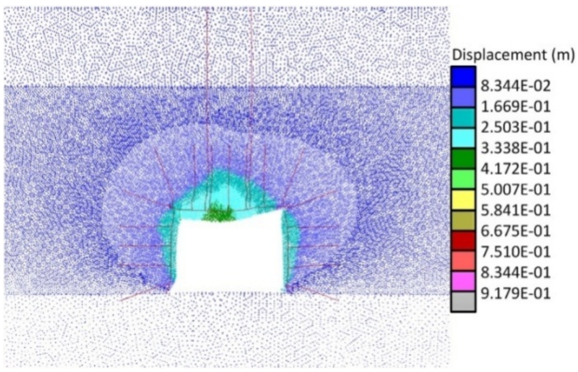

Fig. 18 Simulated displacement vector map of the surrounding rock along the roadway under supported conditions

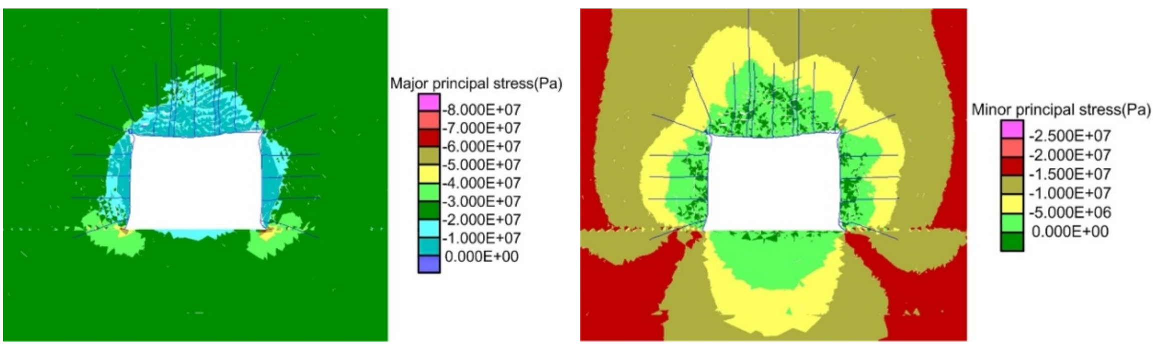

(a) Major principal stress distribution (b) Minor principal stress distribution

Fig. 19 Simulated principal stress distribution around the 1308 gate-road under supported condition

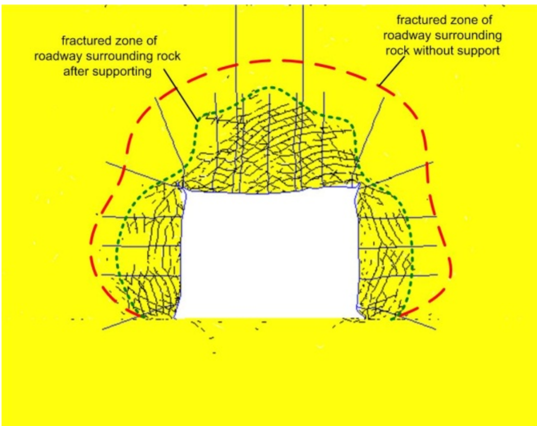

Fig. 20 Comparison of the simulated fracture zone range of the roadway before and after the support

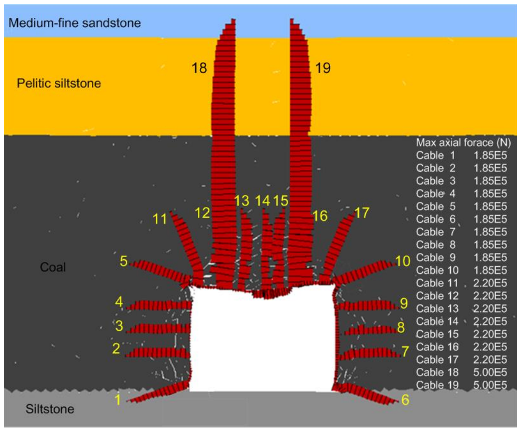

Fig. 21 Simulated stress state of the support elements

5.4 Applications at the 1308 gate-road

The surface convergences of the 1308 gate-road during excavation were monitored to test the supporting effect of the combined support system; the locations of the two monitoring sections are shown in Fig. 1(b). The monitoring results of station #1 (Fig. 22) indicate that the convergence increased quickly within the first 12 days after excavation because of stress release. Thereafter, the deformation was effectively controlled as the support elements controlled the surrounding rock and slowed down any increases in deformation. After excavation for 45 days, the surrounding rock basically became stable. The final roof-to-floor and wall-to-wall convergences were 130 mm and 101 mm, respectively, which were in the allowable range. Compared to the simulation results, the convergences of the surrounding rock were much smaller because the monitoring equipment was installed after the installation of a permanent support, so any convergence before this support could not be monitored. Engineering practices at the 1308 gate-road indicated that the supporting effect of a combined support system was acceptable, as seen in Fig. 23.

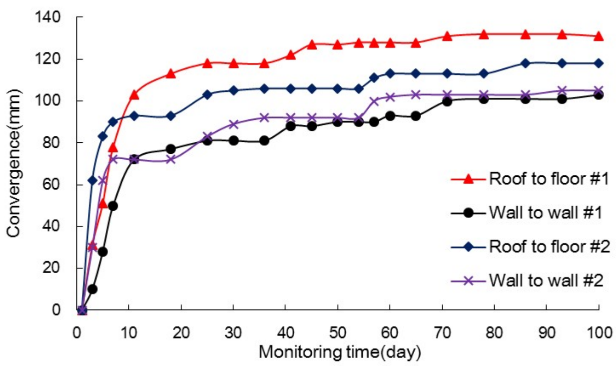

Fig. 22 Relationship curve between the convergence and time of the 1308 gate-road during excavation

Fig. 23 Photograph of the 1308 gate-road that shows a successful reinforcement

6. Conclusions

Deep coal roadways with large sections and thick top coal are widely used by many coal mines in China. The large burial depth, large cross section and low strength of the surrounding rock increase the difficulty of stability control. This study employed the UDEC to investigate the failure mechanisms and stability control mechanisms of this type of roadway. A numerical model was established with innovative UDEC trigon blocks under the background of the 1308 gate-road at the Dongtan coal mine, and the parameters were calibrated to obtain the microscopic parameters in the UDEC from the laboratory test results.

The numerical results show that deformation along the roof was more serious than that in the sides and floor, especially in the center of the roof. Radial stress release was more severe than tangential stress release, while tangential stress concentrated in zones along the roadway. The principal stress distribution show that the areas near the roadway surface exhibited larger tensile stress from excavation. The failure process began from partial failure at the roadway's corners and then propagated deeper into the roof and sides, finally resulting in large deformation along the roadway. The final failure patterns included collapses in the roof and rib spalling in the sides. Therefore, the center of the roof is a critical area to support for such roadways, and the confining pressure should be increased to improve the strength of the surrounding rocks and decrease deformation.

A combined support system was proposed based on the modeling results, which included high-strength, high pre-tension bolts and cables, a T-type roof channel and a wire mesh. The numerical simulation and engineering practice results proved that the combined support system could effectively control the deformation in the surrounding rocks, which could provide references for studies of surrounding rock failure processes and control technology along roadways.

Acknowledgments

This research was supported by the National Natural Science Foundation of of Jiangsu Province for Distinguished Young Scholars (BK20150005), National Nature Science Foundation of China (41272344), the Fundamental Research Funds for the Central Universities (China University of Mining and Technology) (2014YC10) and the Innovation Project of Jiangsu Province

(KYLX16_0538). We also would like to express our sincere gratitude to the editor and two reviewers for their valuable comments, which have greatly improved this paper.

References

Boon, C.W., Houlsby, G.T. and Utili, S. (2015), "Designing tunnel support in jointed rock masses via the DEM", *Rock. Mech. Rock. Eng.*, **48**(2), 603-632.

Brady, B.H.G. and Brown, E.T. (2006), *Rock Mechanics for Underground Mining*, (3nd Ed.), Springer Science and Business Media, New York, NY, USA.

Chen, X.G., Zhang, Q.Y., Wang, Y., Li, S.C. and Wang, H.P. (2013), "In situ observation and model test on zonal disintegration in deep tunnels", *J. Test. Eval.*, **41**(6), 1-11.

Christianson, M., Board, M. and Rigby, D. (2006), "UDEC simulation of triaxial testing of lithophysal tuffs", *Proceedings of the 41st U.S. Rock on Rock Mechanics Symposium*, Alexandria, USA, June.

Gao, F.Q. and Stead, D. (2014), "The application of a modified Voronoi logic to brittle fracture modelling at the laboratory and field scale", *Int. J. Rock. Mech. Min. Sci.*, **68**, 1-14.

Gao, F.Q., Stead, D. and Kang, H. (2014a), "Numerical simulation of squeezing failure in a coal mine roadway due to mining-induced stresses", *Rock Mech. Rock Eng.*, **44**(9), 1-11.

Gao, F.Q., Stead, D. and Kang, H. (2014b), "Simulation of roof shear failure in coal mine roadways using an innovative UDEC Trigon approach", *Comput. Geotech.*, **61**, 33-41.

He, M.C. (2011), "Physical modeling of an underground roadway excavation in geologically 45° inclined rock using infrared thermography", *Eng. Geol.*, **121**(3), 165-176.

He, M.C., Gong, W.L., Zhai, H.M. and Zhang, H.P. (2010a), "Physical modeling of deep ground excavation in geologically horizontal strata based on infrared thermography", *Tunn. Undergr. Sp. Tech.*, **25**(4), 366-376.

He, M.C., Jia, X., Gong, W.L. and Faramarzi, L. (2010b), "Physical modeling of an underground roadway excavation in vertically stratified rock using infrared thermography", *Int. J. Rock. Mech. Min. Sci.*, **47**(7), 1212-1221.

Itasca Consulting Group, Inc. (2004), UDEC–Universal distinct element code; Version 4.0 Manual, Itasca Consulting Group, Inc., Minneapolis, MN, USA.

Jing, L.R. (2003), "A review of techniques, advances and outstanding issues in numerical modelling for rock mechanics and rock engineering", *Int. J. Rock. Mech. Min. Sci.*, **40**(3), 283-353.

Jing, L.R. and Hudson, J.A. (2002), "Numerical methods in rock mechanics", *Int. J. Rock. Mech. Min. Sci.*, **39**(4), 409-427.

Jing, H.W., Yang, S.Q., Zhang, M.L., Xu, G.A. and Chen, K.F. (2014), "An experimental study on anchorage strength and deformation behavior of large-scale jointed rock mass", *Tunn. Undergr. Sp. Tech.*, **43**, 184-197.

Kang, H.P. (2014), "Support technologies for deep and complex roadways in underground coal mines: A review", *Int. J. Coal Sci. Technol.*, **1**(3), 261-277.

Kang, H.P., Lin, J. and Fan, M.J. (2015), "Investigation on support pattern of a coal mine roadway within soft rocks – A case study", *Int. J. Coal Geol.*, **140**, 31-40.

Karampinos, E., Hadjigeorgiou, J., Hazzard, J. and Turcotte, P. (2015), "Discrete element modelling of the buckling phenomenon in deep hard rock mines", *Int. J. Rock. Mech. Min. Sci.*, **80**, 346-356.

Kazerani, T. (2013), "Effect of micromechanical parameters of microstructure on compressive and tensile failure process of rock", *Int. J. Rock. Mech. Min. Sci.*, **64**, 44-55.

Kazerani, T. and Zhao, J. (2010), "Micromechanical parameters in bonded particle method for modelling of brittle material failure", *Int. J. Numer. Anal. Met.*, **34**(18), 1877-1895.

Li, S.J., Yu, H., Liu, Y.X. and Wu, F.J. (2008), "Results from in-situ monitoring of displacement, bolt load, and disturbed zone of a powerhouse cavern during excavation process", *Int. J. Rock. Mech. Min. Sci.*, **45**(8), 1519-1525.

Li, S.C., Wang, Q., Wang, H.T., Jiang, B., Wang, D.C., Zhang, B., Li, Y. and Ruan, G.Q. (2015), "Model test study on surrounding rock deformation and failure mechanisms of deep roadways with thick top coal", *Tunn. Undergr. Sp. Tech.*, **47**, 52-63.

Meguid, M.A., Saada, O., Nunes, M.A. and Mattar, J. (2008), "Physical modeling of tunnels in soft ground: A review", *Tunn. Undergr. Sp. Tech.*, **23**(2), 185-198.

Meng, X.J. (2013), "Surrounding rock control theory and technology of large-section entry driving along goaf in fully mechanized caving face when deep mining", Ph.D. Dissertation; Shandong University of Science and Technology, Qingdao, China. [In Chinese]

Shen, B.T. (2014), "Coal Mine Roadway Stability in Soft Rock: A Case Study", *Rock. Mech. Rock. Eng.*, **47**(6), 2225-2238.

Shen, B.T., King, A. and Guo, H. (2008), "Displacement, stress and seismicity in roadway roofs during mining-induced failure", *Int. J. Rock. Mech. Min. Sci.*, **45**(5), 672-88.

Singh, M. and Seshagiri, R.K. (2005), "Empirical methods to estimate the strength of jointed rock masses", *Eng. Geol.*, **77**(1), 127-137.

Tan, X. and Konietzky, H. (2014), "Brazilian split tests and numerical simulation by discrete element method for heterogeneous gneiss with bedding structure", *Chinese Journal of Rock Mechanics and Engineering*, **33**(5), 938-946. [In Chinese]

Yang, S.Q. (2015), "An experimental study on fracture coalescence characteristics of brittle sandstone specimens combined various flaws", *Geomech. Eng., Int. J.*, **8**(4), 541-557.

Yang, S.Q., Jiang, Y.Z., Xu, W.Y. and Chen, X.Q. (2008), "Experimental investigation on strength and failure behavior of pre-cracked marble under conventional triaxial compression", *Int. J. Solids Struct.*, **45**(17), 4796-4819.

Zhang, L. and Einstein, H.H. (2004), "Using RQD to estimate the deformation moduli of rock masses", *Int. J. Rock. Mech. Min. Sci.*, **41**(2), 337-341.

CC